Surface Adsorption Affects the Performance of Alkaline Anion-Exchange Membrane Fuel Cells

Sandip Maurya[a†], Joseph H. Dumont[a†], Claudia Narvaez Villarrubia[a], Ivana Matanovic[bc], Dongguo Li[a], Yu Seung Kim[a,*], Sangtaik Noh[d], Junyoung Han[d], Chulsung Bae[d], Hamish A. Miller[e], Cy H. Fujimoto[f], and Dario R. Dekel[g,*]

[a] MPA-11: Materials Synthesis & Integrated Devices, Los Alamos National Laboratory, Los Alamos, NM 87545, USA

[b] Department of Chemical and Biological Engineering, Center for Micro-Engineered Materias (CMEM), The University of New Mexico, Albuquerque, New Mexico 87231, USA

[c] Theoretical Division, Los Alamos National Laboratory, Los Alamos, NM 87545, USA

[d] Department of Chemistry and Chemical Biology, Rensselaer Polytechnic Institute, Troy, New York 12180, USA

[e] Istituto di Chimica dei Composti Organometallici (CNR-ICCOM), via Madonna del Piano 10, 50019 Sesto Fiorentino, Firenze, Italy

[f] Materials Science and Engineering Center, Sandia National Laboratories, Albuquerque, New Mexico 87185, USA

[g] The Wolfson Department of Chemical Engineering, Technion – Israel Institute of Technology, Haifa 3200003, Israel

[†] Equal Contributors

*E-mail: yskim@lanl.gov, dario@technion.ac.il

ABSTRACT

Material interactions at the polymer electrolytes-catalyst interface play a significant role in the catalytic efficiency of alkaline anion-exchange membrane fuel cells (AEMFCs). In this work, the surface adsorption behaviors of the cation-hydroxide-water and phenyl groups of polymer electrolytes on palladium-based catalysts are investigated using two Pd-based hydrogen oxidation catalysts – Pd/C and Pd/C-CeO_2 and two Pt-based catalysts – Pt/C and Pt-Ru/C. The rotating disk electrode study and complimentary density functional theory calculation indicate that relatively low co-adsorption of cation-hydroxide-water of the Pd-based catalysts enhances the hydrogen oxidation activity, yet substantial hydrogenation of the surface adsorbed phenyl groups reduces the hydrogen oxidation activity. The adsorption-driven interfacial behaviors of the Pd-based catalysts correlate well with the AEMFC performance. This study gives insight into potential use of non-Pt HOR catalysts which have different surface adsorption characteristics in advanced AEMFCs.

Introduction

Alkaline anion-exchange membrane fuel cells (AEMFCs) is an attractive alternative to acidic proton exchange membrane fuel cells due to the potential use of inexpensive non-precious metal group (non-PGM) catalysts.[1] One of the most significant challenges in this technology is the development of AEMFCs with improved cell performance. Although substantial progress on AEMFC performance has been made in the past years to demonstrate over 1 W cm^{-2} power density, there is still a lack of understanding on the limiting factors that affect cell performance.

The performance of AEMFCs are largely influenced by the hydrogen oxidation reaction (HOR) activity of the AEMFC anode electrode. Yang's group suggested that the HOR kinetics of Pt in alkaline electrolytes are two orders of magnitude slower than in acid electrolyte.[2] Several explanations for the slow HOR kinetics have been proposed,[3-7] including a comprehensive study that recently reviewed the current understanding of HOR electrocatalysis in alkaline media[8]. Based on the HOR mechanistic studies, advanced HOR catalysts having higher HOR activity in alkaline medium have been developed for the AEMFC anode. [9-11]

One significant challenge in developing HOR catalysts by measuring their inherent kinetic activities is the inability to correlate the catalyst activity with the AEMFC performance. For example, the peak power density of current H_2/O_2 AEMFC performance using Pt-based catalysts vary from ~300 mW cm^{-2} to 1,900 mW cm^{-2}, with current densities changing from 40 to 612 mA cm^{-2} at 0.8 V.[12-13] At the highest performance cell, e.g. 612 mA cm-2 at 0.8 V[13], relatively low activity of alkaline anode catalysts appears to no longer be a critical performance limiting factor. The approach of comparing different HOR catalysts by only considering their inherent kinetic activity has even greater limitations for the correlation with AEMFC durability. Most AEMFCs still show a substantial reduction in performance in the first 100–200 hours of operation,[14] while most Pt group metal catalysts are known to be stable under AEMFC operating conditions.[15]

Another critical factor that may significantly impact the AEMFC performance is the catalyst-absorbate/adsorbate-electrolyte interaction. The molecular constituents of polymer

electrolytes such as phenyl and ionic groups can affect the HOR activity of electrocatalysts. It was recently shown that phenyl group adsorption parallel to the catalyst surface seems to be the most significant limiting factor in AEMFC performance.[16] We have demonstrated a three times peak power density improvement with current densities changing from 110 mA cm^{-2} to 430 mA cm^{-2} at 0.8 V of an AEMFC by reducing the phenyl-group adsorption onto anode catalysts.[17] Cumulative co-adsorption of cation-hydroxide-water on the HOR catalyst surface is another factor that limits the cell performance and durability.[18-21] A recent study showed that a cumulative co-adsorption of cation-hydroxide-water occurred at HOR potentials, *ca.* 0.1 V vs. RHE [Reversible Hydrogen Electrode], blocks hydrogen access to the Pt surface.[21] Neutron reflectometry experiments confirmed that the thickness of co-adsorbed layer with high hydroxide concentration (~10.5 M) reached ~15 Å after exposure the Pt electrode for 10 h at 0.1 V vs. RHE.[22]

During our continuous studies on the catalyst-electrolyte interface in the AEMFC anodes, we have paid attention to Pd-based HOR catalysts. Pd catalysts have been considered as alternative catalysts to Pt-based catalysts due to their high HOR activities. In the previous report, a PdNi catalyst exhibited reasonably good performance (125 mA cm^{-2} at 0.8 V; 400 mW cm^{-2} peak power density).[23] Recently, a Pd/C-CeO_2 anode catalyzed AEMFC exhibited 150 mA cm^{-2} at 0.8 V and 500 mW cm^{-2} peak power density under dry H_2 and pure air conditions.[24-25] More recently, the same group further ramped up the performance to 500 mA cm^{-2} at 0.8 V and 1,000 mW cm^{-2} peak power density.[26] One interesting note from the previous research[24] is the Pd/C-CeO_2 anode catalyzed AEMFC performance leads to a fivefold increase in the anode performance relatively to a Pd/C catalyst, which was ascribed to the weakened Pd-H bond that assists in supplying OH_{ad} from oxophilic CeO_2 to the Pd-H_{ad}.

Here, we thoroughly investigate the adsorption characteristics of the Pd-based HOR catalysts by combining rotating disk electrode (RDE), density functional theory (DFT) calculation and AEMFC tests. The purpose of this study is to explore how the adsorption characteristics of the Pd-catalysts impact the AEMFC performance. The adsorption characteristics of commercial Pt/C and Pt-Ru/C catalysts are also provided to compare the HOR activity and AEMFC performance in order to give an insight into the potential use of the non-Pt HOR catalysts in advanced AEMFCs.

Experimental

Catalysts.

Pt/C (60 wt.%, HISPEC® 9100) and Pt-Ru/C (Pt: 50 wt.%, Ru: 25 wt.%, HISPEC® 12100) were purchased from Johnson Matthey Fuel Cells (USA).

Pd/C (10 wt.% Pd) catalyst was prepared by the previously described procedure.[24] Vulcan XC-72 carbon (4.5 g) was suspended in ethylene glycol (250 ml) and a mixture of water (50 ml), ethylene glycol (50 ml) and 37% HCl (6 ml) with $PdCl_2$ (445 mg) precursor was added. A NaOH solution (5 %) and ethylene glycol (35 ml) was introduced in the reactor and reduced the $PdCl_2$ at 125 °C for 3 h under N_2 atmosphere. The solid product was filtered off and washed with water. The final product was dried in vacuum oven at 40 °C.

Pd/C-CeO_2 (10 wt% Pd) catalyst was prepared by the previously described procedure.[24] We first prepared the C-CeO_2 catalyst supporting material. Vulcan XC-72 (4 g) was added to a solution of $Ce(NO_3)_3$ $6H_2O$ (5.31 g) in water (250 ml). After stirring for 30 min and sonication for 30 min, the pH of the mixture was adjusted to 12 by adding 2 M KOH. The solid product was separated by filtration and washed with water until neutral pH. The product was dried at 65 °C and subsequently heated under air in a tube furnace at 250 °C for 2 h. The obtained C-CeO_2 (4 g) was suspended in water and a solution of K_2PdCl_4 (1.38 g, 4.23 mmol) in water (60 ml) was slowly added under vigorous stirring, followed by an aqueous solution of 2.5 M KOH (8.4 ml). Ethanol (50 ml) was added to the mixture and heated to 80 °C for 60 min. The Pd/C-CeO_2 was filtered off, washed several times with distilled water and dried under vacuum at 40 °C.

Rotating Disk Electrode Measurement

Catalyst inks were prepared using Pt/C (60 wt%, HISPEC® 9100) and Pt-Ru/C (Pt: 50 wt%, Ru: 25 wt.%, HISPEC® 12100) from Johnson Matthey Fuel Cells (USA) and two Pd-based catalysts described above. 5 mg of catalyst was mixed in 4 ml of deionized water, 20 µl of Nafion 5 wt. % (Nafion D521 5wt%, Alfa-Aesar, Ward Hill, MA) and 100 µl isopropanol (ACS certified - Fisher Scientific, Fair Lawn, NJ). The mixture was sonicated for 1 hour prior to electrode preparation. Volume of inks were dropped on the RDE to load 20 μg_{metal} cm^{-2} and left to dry at room temperature (25 ± 1 °C).

RDE measurements were performed using a multichannel potentiostat VMP-3, from Biologic Instruments (Pariset, France) in a standard three-electrode cell at room temperature. A graphite rod served as a counter electrode and an Hg/HgO (Radiometer Analytical Inc.) in 1.0 M KOH as a reference electrode for alkaline electrolytes. All potentials initially measured vs. the Hg/HgO electrode were converted to a RHE scale by measuring HOR/hydrogen evolution reaction (HER) currents on the Pt/C, Pt-Ru/C, Pd/C and Pd/C-CeO_2 catalysts in the 0.1 M NaOH, tetramethyl ammonium hydroxide (TMAOH) and benzyltrimethyl ammonium hydroxide (BTMAOH), whereby the potential at zero current corresponds to 0.0 V *vs*. RHE.

The electrodes were stabilized by cyclic voltammograms at 100 mV s^{-1} between 0.0 and 1.2 V *vs.* RHE in electrolytes saturated with nitrogen. Later, in electrolytes saturated with pure hydrogen, all electrodes were preconditioned at 1.4 V for 30 seconds to remove any cations[19] and polarization plots were recorded between *ca*. −0.1 and 1.2 V *vs*. RHE at a sweep rate of 5 mV s^{-1} and rotation rate of 900 rpm. Next, cyclic voltammogram was recorded between 0.0 and 1.2 V vs. RHE at a scan rate of 20 mV s^{-1} at 0 rpm, after the same preconditioning step. The AC impedance was measured from 100 to 0.001 kHz with a voltage perturbation of 5 mV in the hydrogen saturated electrolytes at 0.1 V vs. RHE. The resistance of the 0.1 M NaOH, TMAOH and BTMAOH are ∼8 Ω, indicating that there is no significant pH effect on our experiments. Chronoamperometric experiments were performed at 0.1 V vs. RHE for 30 minutes, after the same preconditioning step, followed by recording of polarization plots as stated above. The RDE measurements were repeated 3-4 times, independently, to ensure data reproducibility. Typical standard deviation of the measured HOR current is 5-10 %.

Polymer Electrolytes.

Quaternized poly(terphenylene) (TPN) synthesized via simple acid-catalyzed Friedel-Crafts polycondensation[27] was used as anion-exchange membrane (AEM). The dry thickness of the TPN AEM was 35 μm. The hexamethyl ammonium tethered Diels-Alder poly(phenylene) (PP-HTMA)[28] and pentamethyl ammonium tethered poly(fluorene) (FLN)[29] [Ref] were used as ionomeric binder for the electrodes. The chemical structure of the membrane and ionomeric binders are shown in **Figure 1**.

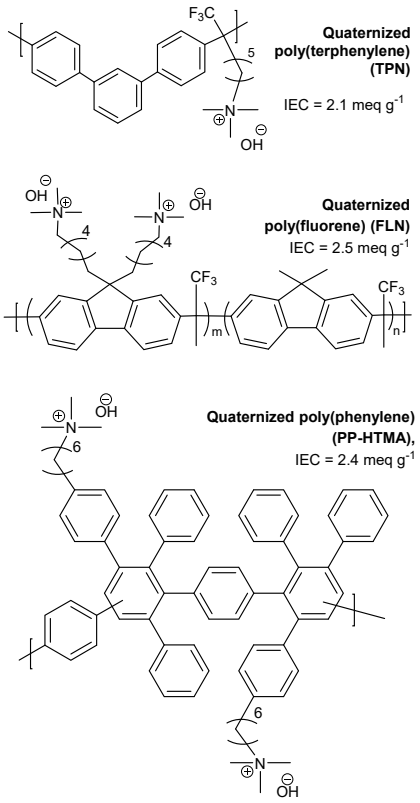

Figure. 1. Chemical structure of the polymer electrolytes used for this study.

Preparation of Membrane Electrode Assembly

Catalyst inks were prepared using Pt-based catalysts as reference (Pt/C, Pt-Ru/C) and two Pd-based catalysts (Pd/C and Pd/C-CeO_2) described above. For cathode catalyst layers, the Pt/C catalyst and FLN ionomer were used for all the membrane electrode assemblies (MEAs). The Pt/C and FLN ionomer were mixed in a water-isopropanol (20:80 vol.%) mixture followed by sonication for 1 h. An I/C ratio (ionomer to catalyst) was kept at 17.3 wt%. For anode catalyst layers, the Pt-Ru/C, Pd/C and Pd/C-CeO_2 catalysts and FLN ionomer were mixed in a water-isopropanol (20:80 vol.%) mixture. The catalyst ink was sonicated at least 1 h for the good dispersion. An I/C ratio (ionomer to catalyst) was kept at 17.3, 33 and 21.33 wt% for Pt-Ru/C, Pd/C and Pd/C-CeO_2 catalysts, respectively. These catalyst inks were painted onto the gas diffusion layers (5 cm^2, BC29, SGL Carbon) on the vacuum table at 60 °C. The metal loadings on the final gas diffusion electrodes (GDEs) were 0.6, 0.75 (0.5 mg_{Pt} + 0.25 mg_{Ru}), 0.15, and 0.15 mg cm^{-2} for Pt/C, Pt-Ru/C, Pd/C and Pd/C-CeO_2, respectively.

For the sake of comparison, Pt/C cathode and Pd/C-CeO_2 anode were prepared using hexamethyl ammonium tethered Diels-Alder poly(phenylene) (PP-HTMA) by mixing catalyst and ionomer in the 20:80 vol. % ethylene glycol-methanol mixture. The I/C ratio and metal loadings were kept similar with the FLN-bonded GDEs for direct comparison.

The prepared GDEs and the TPN membrane were then converted to hydroxide form by immersing them in 1 M NaOH solution. The AEM was then sandwiched between the cathode/anode GDEs and placed into the fuel cell hardware (5 cm^2, serpentine flow field, Fuel Cell Technologies, Inc., USA).

Fuel Cell Testing

The cell temperature was raised to 80 °C before flowing reactant gases. Then, 100% RH H_2/O_2 gases were flowed into the cell at 2000 sccm and 1000 sccm, respectively. The polarization curves after break-in at 0.5 V for 24 h were acquired at absolute backpressures ranging from 78 or 285 kPa using a fuel cell station (Fuel Cell Technologies Inc., USA.)

Life test was performed at constant current density of 0.6 A cm^{-2}. The cell was operated at 80 °C, 147 kPa backpressure with flowing H_2 (2000 sccm) and O_2 (300 sccm) under fully humidified conditions. During the life test, (bi)carbonate ions from the humidified water was built-up in the AEM, which increases the cell resistance [30-31]. To avoid carbonation process to occur during the life-test the cell was replenished as needed. For the replenishing process, the cell operation was halted and the cell temperature was lowered to room temperature. 1 M NaOH was flowed in to the single cell then the cell is rinsed until the effluent water from electrodes was neutral. After the replenishing, the cell temperature was increased to 80 °C and continued the life test under the same conditions described above.

DFT Calculations

The density functional calculations (DFT) were performed using Perdew-Wang 91 (PW91)[32-33] exchange-correlation functional and projector augmented-wave pseudopotentials [34-35] as implemented in the Vienna Ab initio simulation package (VASP)[36-39]. Extended Pd(111) surface was modeled using a super cell with the dimensions of 16.46 Å x 16.46 Å, respectively. These correspond to the unit cells of the size $(3a\sqrt{2} \times 3b\sqrt{2})R\gamma=60°$ where $a=b=3.88$ Å are the experimentally determined cell parameters (ICSD 64915). Hydrogen

covered Pd(111) surface was modelled using the 0.33 monolayer (ML) coverage of hydrogen adsorbed in hcp position[40]. In all the cases we modeled the system using three layers of metal atoms and a vacuum region of 20 Å. To simulate the effect of the bulk, the two top layers and the adsorbed species were allowed to relax while the bottom layers were held fixed. The electronic energies were calculated using 4x4x1 k-point Monkhorts-Pack[41] mesh and Methfessel-Paxton smearing [42] of order 2 with σ =0.2. Plane-wave basis cutoff was set to 400 eV. The change in the free energy during the adsorption was calculated as

$$\Delta rG = \Delta E_{\mathrm{ad}} + \Delta ZPE + T\Delta S$$

where ΔE_{ad}, ΔZPE, and ΔS are the change in the electronic energy, zero point energy, and entropy. Adsorption energy was calculated using the following formula:

$$\Delta E_{\mathrm{ad}} = E_{\mathrm{surface+ad}} - [E_{\mathrm{surface}} + E_{\mathrm{ad}}]$$

where $E_{\mathrm{surface+ad}}$ is the energy of the cation/phenyl adsorbed on the Pd(111) surface or Pd(111) surface with 0.33 ML coverage of hydrogen, E_{surface} is the energy of the clean surface, and E_{ad} is the energy of the cation/phenyl in the gas phase. Zero point energy and the entropy values were previously calculated as explained in Ref [16].

Results and Discussion

Co-adsorption of cation-hydroxide-water

The morphological characterization of the as-synthesized Pd/C and Pd/C-CeO_2 catalysts can be found in previous publications.[24-25] The co-adsorption of cation-hydroxide-water on the surface of the HOR catalysts is investigated through the RDE measurements in 0.1 M TMAOH. **Figure 2a** shows the HOR voltammograms of the different catalysts obtained from the anodic scans from −0.1 to 1.2 V *vs.* RHE in hydrogen-saturated solution after the preconditioning at 1.4 V for 30 sec, the voltage at which the TMA cations are desorbed from the catalyst surface.[19] The HOR voltammograms of Pt/C and Pt-Ru/C exhibit a very similar shape. In contrast, the voltammogram of Pd/C features a peak in the oxidation current at *ca.* 0.3 V that is likely caused by the hydrogen absorption that can be accomplished under electrochemical conditions near 0 V. [43-45] Desorption of the absorbed hydrogen (H_{abs}) takes place at potentials higher that the onset potential of HOR, thus large anodic current associated with the desorption of H_{abs} overlap anodic currents in HOR voltammograms

associated with surface processes. The HOR voltammogram of Pd/C-CeO_2 shows the peak at ~ 0.3 V but the peak was much smaller than that of Pd/C. This suggests that the hydrogen absorption for the Pd/C-CeO_2 catalyst may be suppressed compared with that for the Pd/C catalyst, probably because the interaction between Pd and CeO_2 weakens the Pd-H bonds[24]. The kinetic current density of Pt/C at 0.01 V measured as a gauge for HOR activity of the Pt/C electrode is 0.18 mA cm^{-2}, slightly lower than that of Pt-Ru/C (0.21 mA cm^{-2}). Despite the current due to H_{abs} was added to the HOR current density of Pd/C, the measured HOR current density of Pd/C at 0.01 V is *ca.* 0.05 mA cm^{-2}, substantially lower than those of Pt/C and Pt-Ru/C. The kinetic current density of Pd/C-CeO_2 is 0.15 mA cm^{-2}, notably better than that of Pd/C.

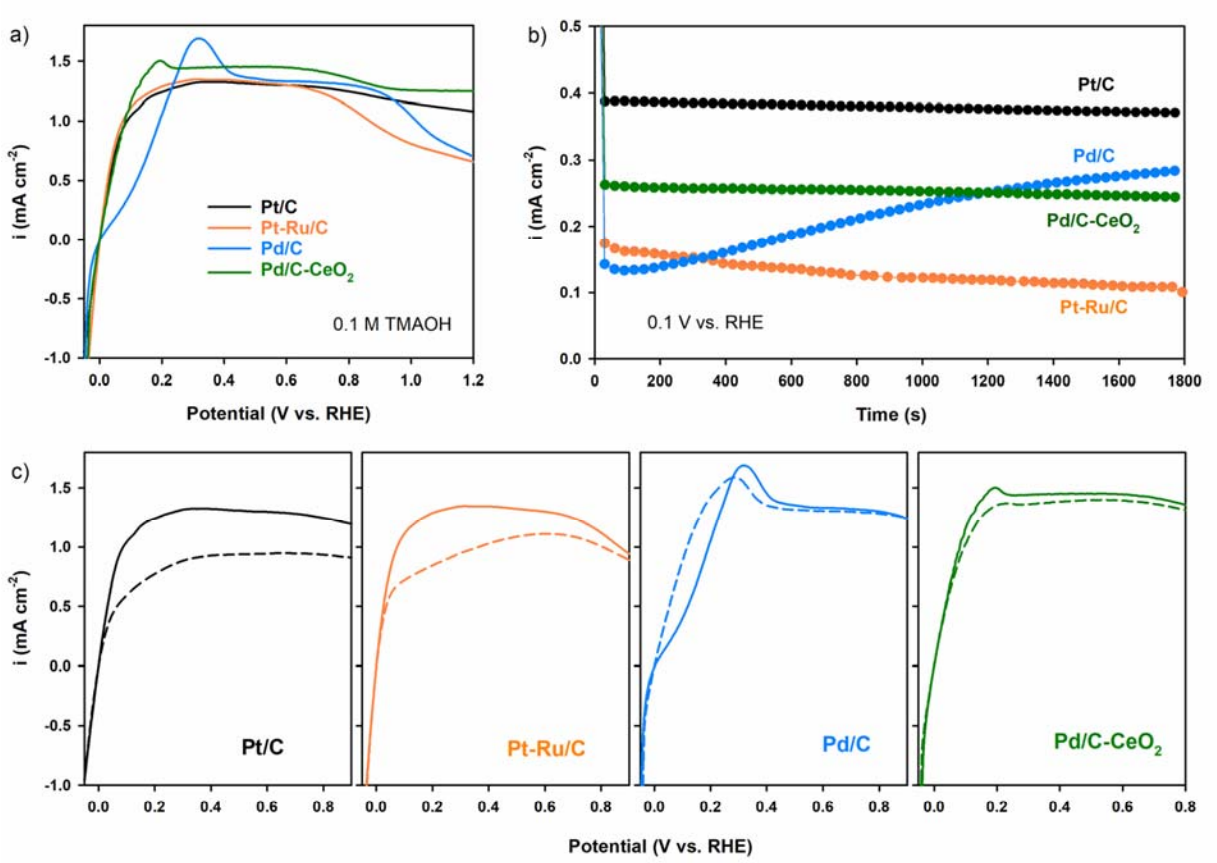

Figure 2. (a) HOR voltammograms of Pt/C, Pt-Ru/C, Pd/C and Pd/C-CeO_2 (metal loading was 20 μg cm^{-2}) in 0.1 M TMAOH (b) Chronoamperometry at 0.1 V vs. RHE. (c) HOR voltammogram comparison before (solid line) and after (dash line) the chronoamperometry. The voltammograms measured at 25 °C; rotating speed, 900 rpm; and scan rate, 5 mV s^{-1}.

Chronoamperometry performed at 0.1 V vs. RHE for 30 min are shown in **Figure 2b**. The initial HOR current density of Pt/C, Pt-Ru/C and Pd/C-CeO_2 constantly decreased over 30 min. The decreasing HOR current density of the Pt-based catalysts is due to the limited hydrogen access by the less hydrogen-permeable cumulative co-adsorbed cation-hydroxide-water layer.[21] In contrast, the HOR current density of Pd/C increased over time.

Figure 2c compares the HOR voltammograms of the catalysts before and after the chronoamperometry. The kinetic current density of Pt/C and Pt-Ru/C at 0.01 V notably decreases from 0.18 and 0.21 mA cm^{-2} to 0.13 and 0.19 mA cm^{-2}, respectively. Much significant decrease in HOR limiting current density is measured. For Pt/C, the limiting current measured at 0.6 V vs. RHE decreases from 1.30 to 0.94 mA cm^{-2}. Similar loss in HOR limiting current density is observed for Pt-Ru/C (1.30 to 1.10 mA cm^{-2}). In sharp contrast, for Pd/C, the kinetic current density at 0.01 V increased from 0.05 to 0.10 mA cm^{-2} after the chronoamperometry experiment. The HOR limiting current density of Pd/C remained same. The kinetic current density and the limiting current density of Pd/C-CeO_2 were similar (0.15 mA cm^{-2}) after the chronoamperometry.

To confirm the peculiar behavior of the Pd/C catalyst, we performed the RDE experiment in NaOH. **Figure S1** shows that the HOR voltammograms before and after chronoamperometry in 0.1 M NaOH. The HOR votammograms of Pt/C exhibit a very similar behavior with those measured in 0.1 M TMAOH: i) the featured peak at 0.3 V, ii) the improved HOR activity and constant HOR limiting current density after the chronoamperometry experiment and iii) the increasing HOR current density during the chronoamperometry experiment. Since a peak in HOR voltammograms often appeared due to the remained hydrogen from excessive hydrogen evolution,[21] we have further investigated the RDE experiment under narrower potential window from 0.0 to 1.2 V vs. RHE. **Figure S2** shows that the peak at 0.3 V derived from hydrogen absorption positively shifted *ca.* ~0.05 V yet the size of the peaks are comparable. This indicates that that the peak appeared in the HOR volatammgram of Pd/C is likely originated from the outstanding hydrogen absorption characteristic of the Pd/C catalyst rather than from the hydrogen evolution. The RDE result suggests that the hydrogen

absorption characteristic of Pd/C evidenced by the peak at 0.3 V may be related to the increase of HOR current density over time.

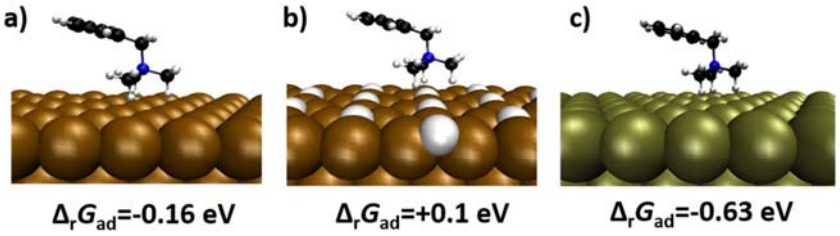

Figure 3. DFT calculated geometries and free energy for the cation adsorption on a) Pd(111), b) Pd(111) with 0.33 ML coverage of H and c) Pt(111).

The RDE result suggests that the hydrogen absorption characteristic of the HOR catalysts is related to the current density change during the chronoamperometry test. Namely, the strong hydrogen absorption of Pd/C can prevent the co-adsorption of cation-hydroxide-water at the HOR potential, which enhances the HOR activity over time by further catalyst activation. The results of DFT calculations (**Figure 3**) show that the adsorption of the cation is indeed weaker on the Pd(111) surface as compared to the Pt(111) surface and is additionally weakened by the H atoms adsorbed on the Pd surface. Moreover, hydrogen adsorption on Pd changes the cation adsorption from an exothermic ($\Delta_r G_{ad}<0$) to an endothermic process ($\Delta_r G_{ad}>0$), confirming that the hydrogen absorption can inhibit cation adsorption on Pd. When compared the two Pd-based catalysts, the HOR voltammograms indicate that Pd/C has stronger hydrogen absorption than Pd/C-CeO_2, probably because the interaction between Pd and CeO_2 weakens the Pd-H bonds[24]. This is consistent with the previous studies[4, 28] that Pd/C has stronger hydrogen binding energy (HBE) than Pd/C-CeO_2. While the Pd/C-CeO_2 catalyst having less HBE exhibits better HOR activity than the Pd/C catalyst before the chronoamperometry test, our study further suggests that the strong hydrogen absorption characteristic of Pd/C may be beneficial for preventing the co-adsorption and improve the hydrogen oxidation process. This section concludes that (1) the initial HOR activity assessed by the HOR current at 0.01 V in 0.1 M TMAOH decreases in the order: Pt-Ru/C (0.21 mA cm^{-2}) > Pt/C (0.18 mA cm^{-2}) > Pd/C-CeO_2 (0.15 mA cm^{-2}) > Pd/C

(0.05 mA cm^{-2}); (2) the cumulative co-adsorption of cation-hydroxide-water is more significant with the Pt-based catalysts than the Pd-based catalysts; and (3) the HOR activity after the 30 min chronoamperometry at 0. 1 V vs. RHE is: Pt-Ru/C (0.19 mA cm^{-2}) > Pd/C-CeO_2 (0.15 mA cm^{-2}) > Pt/C (0.13 mA cm^{-2}) > Pd/C (0.10 mA cm^{-2}).

Phenyl group adsorption

The impact of phenyl group adsorption on the HOR activity is investigated by the RDE experiment with BTMAOH. BTMAOH is one of the most popular cationic groups used for alkaline membranes.[46-49] Our previous study elucidated that the current density suppression of Pt catalysts is due to the adsorption of phenyl group of BTMAOH onto the catalyst surface.[16] The adsorption energies of phenyl group on Pd(111), hydrogen covered Pd(111) and Pt(111) surface were first calculated by DFT (**Figure S3**). The DFT results show that (1) the phenyl group adsorption is stronger on Pt(111) than Pd(111), (2) the adsorption of phenyl group is less favorable with hydrogen covered Pd(111) than with Pd(111), (3) the phenyl group adsorption is, however, still an energetically favorable process even with the hydrogen covered Pd(111), which is in contrast with Pt-Ru catalyst that the phenyl group adsorption is endergonic ($\Delta_r G_{ad}$ = +0.20 eV).[16]

Figure 4a compares the HOR voltammograms of Pt/C, Pt-Ru/C, Pd/C and Pd/C-CeO_2. The HOR curve of Pt-Ru/C is similar to that measured in 0.1 M TMAOH. However, the HOR current density of Pt/C in 0.1 M BTMAOH starting from 0.05 V was markedly suppressed before reaching the limiting value. In our previous report, it was elucidated that the suppressed HOR current density was due to the plenary adsorption of the phenyl group.[16] For Pd/C and Pd/C-CeO_2, the HOR current density is missing at low potentials and the positive current density only appeared at the potential of above 0.31 V (for Pd/C-CeO_2) and 0.39 V (for Pd/C) *vs.* RHE. This negative current density at a positive potential cannot simply be explained by the phenyl group adsorption but may be related with the hydrogenation of the adsorbed phenyl group that may occurs more substantially with Pd-based catalysts[50]. **Figure 4b** and **c** show that CVs of the Pd-based catalysts. The CV of the Pd/C catalyst in NaOH shows a well-defined hydrogen adsorption-desorption regions. The CV in TMAOH shows similar hydrogen adsorption-desorption regions but the desorption peaks are less significant. The CV of the Pd/C catalyst in BTMAOH does not show the hydrogen adsorption-

desorption peaks due to the substantial hydrogenation current of the adsorbed phenyl group. The cyclic voltammograms of Pd/C-CeO_2 show similar changes with those of Pd/C, yet the overall hydrogen adsorption and desorption areas in NaOH and TMAOH solutions were much smaller due to the less hydrogen absorption characteristics of Pd/C-CeO_2.

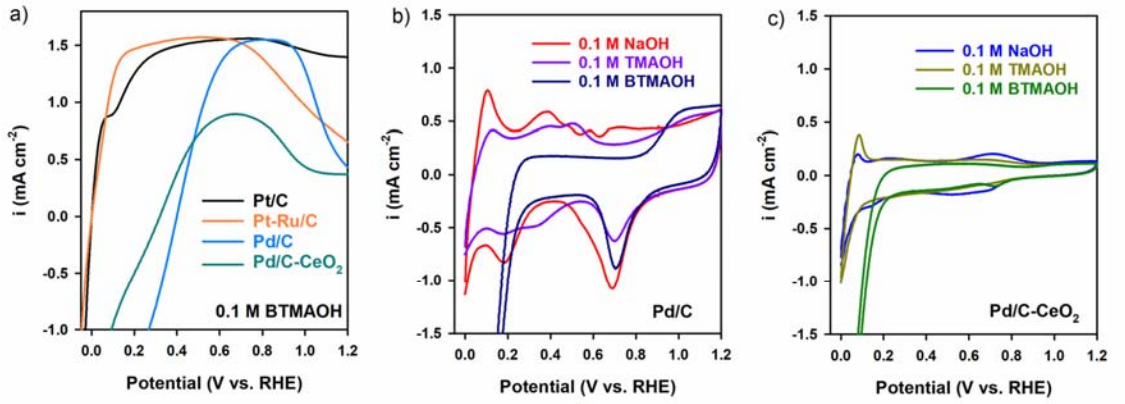

Figure. 4. RDE experiment in 0.1 M BTMAOH (a) HOR voltammograms of Pt/C, Pt-Ru/C, Pd/C and Pd/C-CeO_2 in 0.1 M BTMAOH electrolyte. The metal loading was 20 μg cm^{-2}. The HOR voltammograms were performed at 25 °C; rotating speed, 900 rpm; and scan rate, 5 mV s^{-1}. CVs of Pd/C (b) and Pd/C-CeO_2 (c) in 0.1 M NaOH, TMAOH and BTMAOH electrolytes. The CVs were obtained at 25 °C; rotating speed, 0 rpm; and scan rate, 20 mV s^{-1}.

The impact of phenyl group adsorption on the co-adsorption of cation-hydroxide-water is further investigate by measuring the HOR voltammograms in BTMAOH before and after the chronoamperometry at 0.1 V vs. RHE for 30 min. **Figure 5a** shows that the kinetic current density of Pt/C after the chronoamperometry is almost same and the limiting current density slightly decreases. Compared to the HOR activity loss of Pt/C in TMAOH, the reduction of HOR current density is notably smaller. Furthermore, the small inflection point at ~0.1 V *vs.* RHE after the chronoamperometry experiment (due to the phenyl group adsorption) diminishes. These results suggest that less co-adsorption of cation-hydroxide-water may occur when phenyl group adsorption takes place. **Figure 5b** shows that the HOR current density of Pt-Ru/C in BTMAOH decreases after the chronoamperometry in the similar degree of that measured in 0.1 M TMAOH (see **Figure 1d**). This is probably due to the least phenyl group adsorbing characteristic of Pt-Ru/C[17] which does not interfere the co-adsorption of cation-hydroxide-water group.

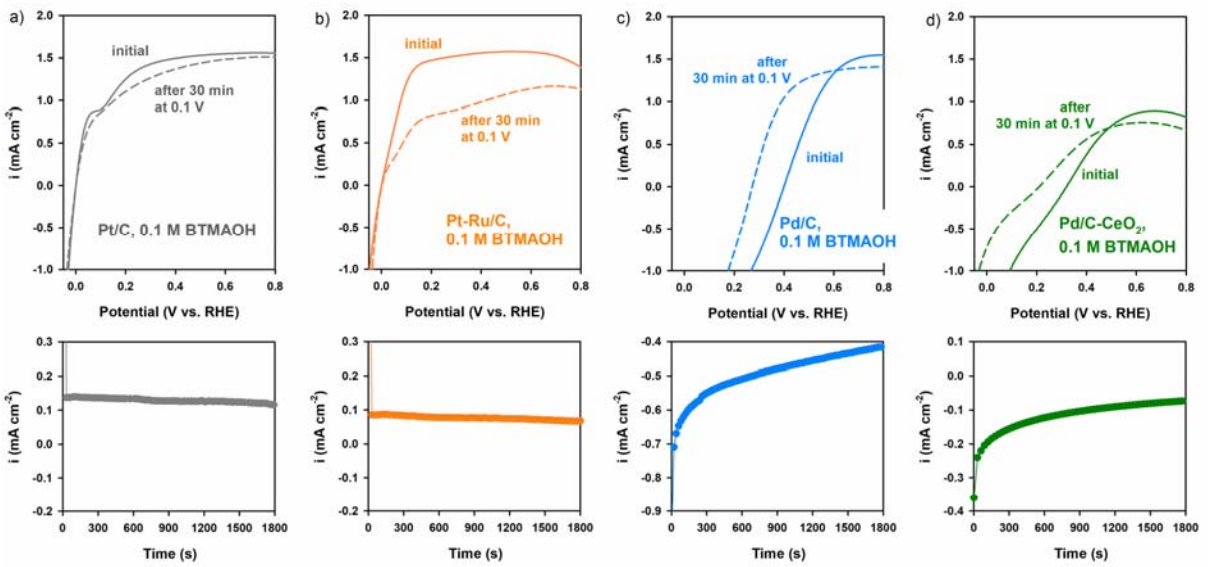

Figure. 5. RDE experiment in 0.1 M BTMAOH. HOR voltammograms of (a) Pt/C, (b) Pt-Ru/C, (c) Pd/C and (d) Pd/C-CeO_2 before (solid line) and after (dashed line) chronoamperometry at 0.1 V. The metal loading was 20 μg cm^{-2}. The HOR voltammograms were performed at 25 °C; rotating speed, 900 rpm; and scan rate, 5 mV s^{-1}. The corresponding chronoamperometry plots shown below were carried out at 0.1 V for 30 min at 900 rpm.

Figure 5c and **d** show the HOR voltammogram changes of the Pd-based catalysts. In both cases, the potential significantly negatively shifted *ca.* –0.15 V and the hydrogenation current density of the phenyl group rapidly decreased during the chronoamperometry. This suggests that the phenyl group adsorption may further prevent the co-adsorption of cation-hydroxide-water. The DFT calculation also support that phenyl group adsorption interferes the co-adsorption of cation-hydroxide-water. The cation adsorption energy of TMAOH on Pd(111) and hydrogen covered Pd(111) is ~ 0.7 eV greater than that of BTMAOH (**Figure S4**). The adsorption interference between phenyl group and cationic group was also shown in the previous DFT study on Pt(111) by a configurational change of the BTMAOH molecules.[16] The high phenyl group adsorbing characteristics of the Pd-based catalysts may lead to a higher HOR activity over time. However, the benefit of using phenyl group containing ionomers with the Pd-based catalysts may not lead AEMFC performance improvement because of the substantial HOR inhibition by the hydrogenation of the adsorbed phenyl groups. This section concludes that (1) the phenyl group adsorption is more significant in the order of Pt/C > Pd/C, Pd/C-CeO_2 > Pt-Ru/C; (2) hydrogenation reaction of the adsorbed phenyl group is observed in the voltammograms of the Pd-based catalysts, and

(3) the phenyl group absorption and co-adsorption of cation-hydroxide-water interfere each other.

Impact on AEMFC performance

We first investigate the impact of phenyl group adsorption on AEMFC performance using two polyaromatic ionomers *ca.* Diels-Alder poly(phenylene) (PP-HTMA) and poly(fluorene) (FLN). From our previous study, it was found that the phenyl groups in PP-HTMA strongly adsorb on the surface of Pt. In contrast, FLN has minimal phenyl group adsorption on Pt-based catalysts as the fluorene unit have the fused five member ring which can prevent the rotation of two phenyl ring.[27]

Figure 6 compares the H_2/O_2 AEMFC performance of Pd/C-CeO_2 anode catalyzed MEAs employing the PP-HTMA and FLN ionomers. All other MEA components as well as the AEMFC operating conditions are identical for all the experiments. Very similar cell HFR between the cells with both ionomers indicates that the membrane hydration through the fuel cell electrodes is similar for both MEAs. The AEMFC using the FLN ionomer exhibited much better performance than that using the PP-HTMA ionomer. The current density at 0.8 V of the MEA using the FLN ionomer reached 260 mA cm^{-2}, 3.5 times higher than that of the MEA using the PP-HTMA ionomer. Likewise, the peak power density of the MEA using the FLN ionomer reached 676 mW cm^{-2}, almost 6 times higher than that of the MEA using the PP-HTMA ionomer. The difference in performance between the two MEAs is much larger than those of MEAs employing Pt/C or Pt-Ru/C which exhibited 2.8 times and 1.5 times performance differences, respectively (**Figure S5**). This indicates that the HOR inhibition by the adsorbed phenyl group and resultant hydrogenation reaction is more pronounced with the Pd-based catalyst than the Pt/C and Pt-Ru/C catalysts. This result suggests that Pd-based catalysts should be incorporated with polymer electrolytes which have low adsorption energy of phenyl groups such as perfluorinated,[51] polyolefinic[52] and poly(fluorene)s[29].

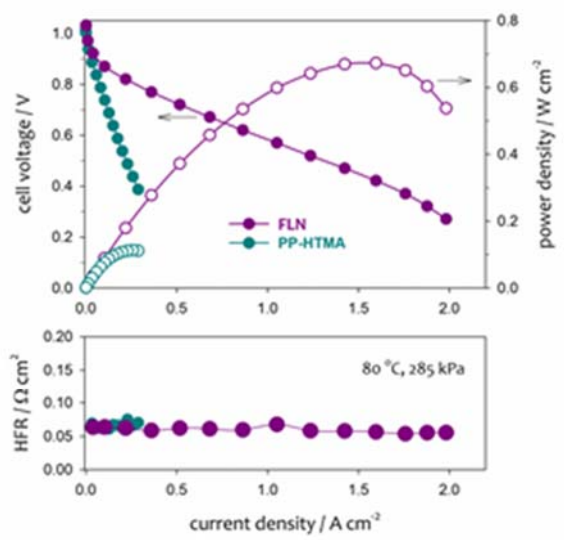

Figure 6. Impact of phenyl group adsorption for Pd/C-CeO_2 anode catalysed AEMFC performance. Two ionomers, PP-HTMA and FLN were used for both anode and cathode. Anode: Pd/C-CeO_2 (0.6 mg_{Pd} cm^{-2}), cathode: Pt/C (0.6 mg_{Pt} cm^{-2}). Measured the AEMFC performance at 80 °C with fully humidified H_2 (2000 sccm) and O_2 (1000 sccm) at 285 kPa backpressure.

Next, we investigate the impact of co-adsorption of cation-hydroxide-water on AEMFC performance. **Figure 7a** shows the AEMFC performance over time of the MEA employing the Pd/C anode catalyst. The AEMFC performance shown here was measured at the ambient pressure as the Pd anode catalyzed MEAs are prone to be flooded at P_{abs} = 285 kPa after the later stage of the life test. The initial cell performance is low with notably high HFR (0.27 Ω cm^2). However, the cell performance kept increasing over time; the peak power density increased from 68 to 360 mW cm^{-2} during 350 h continuous operation. This is because the initial performance of the Pd/C catalyzed MEA was adversely affected by the strong HBE, yet the hydrogen absorption characteristic gives a positive impact on the AEMFC performance by preventing the co-adsorption of cation-hydroxide-water during the continuous cell operation. **Figure 7b** shows the AEMFC performance over time of the MEA employing the Pd/C-CeO_2 anode catalyst. The MEA employing the Pd/C-CeO_2 anode catalyst at 0 h outperforms the MEA employing the Pd/C anode catalyst. The peak power density of the Pd/C-CeO_2 anode catalyzed MEA was 350 mW cm^{-2}, four times greater than that of the Pd/C

anode catalyzed MEA (peak power density: 141 mW cm^{-2}). The superior performance of the Pd/C-CeO_2 catalyzed MEA to the Pd/C catalyzed MEA is consistent with the previous result that also showed approximately five times greater peak power density was obtained with the Pd/C-CeO_2 anode catalyzed MEA.[24] However, by preventing the co-adsorption of cation-hydroxide-water during the cell operation, the performance of the Pd/C catalyzed MEA increased over time. The comparable AEMFC performance obtained with Pd/C catalyst cannot be explained by HBE alone without considering the adsorption behavior.

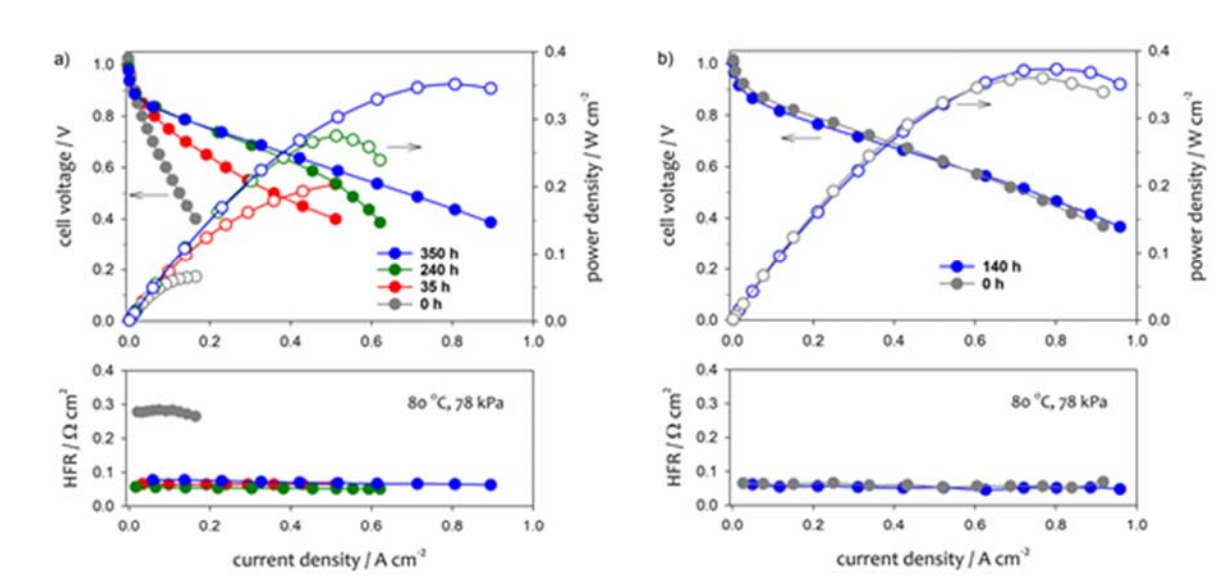

Figure 7. The change of AEMFC performance of MEAs using (a) Pd/C and (b) Pd/C-CeO_2 anode catalyst over time. Measured the H_2/O_2 AEMFC performance at 80 °C at 78 kPa (Los Alamos ambient pressure) after continuous H_2/O_2 AEMFC operation at 80 °C. Ionomer: FLN. The cell performance at 0 h was measured after 12 h cell break-in at 80 °C under constant voltage of 0.6 V.

Figure 8 compares the AEMFC performance of Pt/C, Pt-Ru/C, Pd/C and Pd/C-CeO_2 anode catalyzed MEAs at 80 °C. For Pt/C, Pt-Ru/C and Pd/C-CeO_2 catalyzed MEAs, the initial cell performance was taken as the AEMFC performance employing those HOR catalysts does not change over time. The performance of Pd/C catalyzed MEA was taken after the operation of 350 h (for ambient pressure) and 55 h (for 285 kPa backpressure) as the performance increased at the times. When the AEMFC performance measured at an ambient pressure (**Figure 8a**), the Pt-Ru/C and Pt/C anode catalyzed MEAs exhibit better performance than Pd/C and Pd/C-CeO_2 anode catalyzed MEAs; the peak power density of the MEAs are for Pt-

Ru/C, Pt/C, Pd/C and Pd/C-CeO_2 are 600, 510, 360 and 380 mW cm^{-2}, respectively. The performance of the MEAs measured at 285 kPa exhibits the similar trend (**Figure 7b**), namely the Pt-Ru/C and Pt/C anode catalyzed MEAs exhibit better performance than Pd-based anode catalyzed MEAs; The peak power density values for the Pt/C, Pt-Ru/C, Pd/C and Pd/C-CeO_2 anode catalyzed MEAs are 1440, 1270, 940 and 670 mW cm^{-2}, respectively. One should note that the peak power density of the Pd/C anode catalyzed MEA reached close to 1 W cm^{-2} although the best kinetic performance of the Pd/C anode catalyzed MEA after the later stage of the fuel cell operation was not able to be measured due to the anode flooding. The AEMFC performance of the four MEAs well reflects the HOR activity measured by RDE in 0.1 M TMAOH; the RDE kinetic current of Pt-Ru/C, Pt/C, Pd/C and Pd/C-CeO_2 were 0.21, 0.18, 0.13 and 0.12 mA cm^{-2}, respectively. These results strongly suggest that the co-adsorption of cation-hydroxide-water is a critical parameter for AEMFC performance when ionomers with little phenyl group adsorption are used in the catalyst layer.

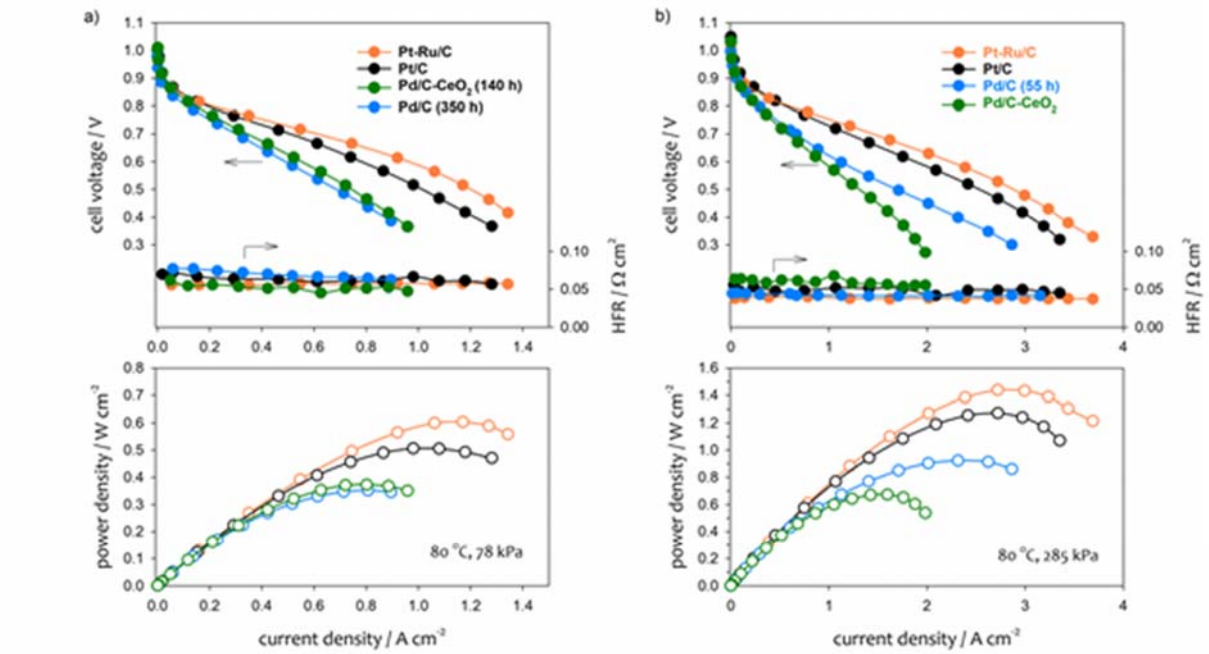

Figure 8. H_2/O_2 AEMFC performance comparison. Measured the AEMFC performance at 80 °C with fully humidified H_2 (2000 sccm) and O_2 (1000 sccm) at (a) 78 kPa (Los Alamos ambient pressure) and (b) 285 kPa anode and cathode backpressure. Membrane: TPN (35 μm thick), Ionomer: FLN. Anode: Pd/C (0.6 mg_{Pd} cm^{-2}), Pd/C-CeO_2 (0.6 mg_{Pd} cm^{-2}), Pt/C (0.6 mg_{Pt} cm^{-2}) or Pt-Ru/C (0.5 mg_{Pt} cm^{-2}) and cathode: Pt/C (0.6 mg_{Pt} cm^{-2}).

Conclusions

By combining RDE, DFT calculation and AEMFC performance tests, we demonstrate that the adsorption of ionomer components on the surface of HOR catalysts play a major role in the AEMFC performance. We elucidated that strong hydrogen absorption characteristic of Pd-based catalysts may prevent the co-adsorption of cation-hydroxide-water which significantly inhibits the hydrogen oxidation process in AEMFCs. This study also shows that Pd-based catalysts is susceptible to the adsorption and hydrogenation of phenyl group; however, incorporating an ionomer that has low phenyl group adsorption energy can minimize the negative impact. The comparative performance study shows that the Pd/C anode catalyzed MEA reached a peak power density close to 1 W cm^{-2} after increasing HOR activity over time, revealing a clear benefit associated with the extraordinary hydrogen absorption characteristics of the Pd/C catalyst.

Acknowledgment

This work was fully supported by the U.S. Department of Energy (US DOE), Office of Energy Efficiency and Renewable Energy (EERE), Fuel Cell Technologies Office (FCTO) under contract no. DE-AC52-06NA25396 (Los Alamos National Laboratory). This work was also partially funded by the Nancy & Stephan Grand Technion Energy Program (GTEP); by the European Union's Horizon 2020 research and innovation program [grant No. 721065]; by the Ministry of Science, Technology & Space of Israel through the M.Era-NET Transnational Call 2015, NEXTGAME project [grant No. 3-12940], and through grant No. 3-12948; by the Israel Science Foundation (ISF) [grant No. 1481/17]; by the Israeli Committee of High Education and the Israeli Prime Minister office via the INREP project; by the Israel Innovation Authority through the KAMIN program [grant No. 60503]; and by the Ministry of National Infrastructure, Energy and Water Resources of Israel [grant No. 3-13671].

References

1. Gottesfeld, S.; Dekel, D. R.; Page, M.; Bae, B.; Yan, Y. S.; Zelenay, P.; Kim, Y. S., Anion Exchange Membrane Fuel Cells - Current Status and Remaining Challenges. *J Power Sources* **2018,** *375*, 170-184.
2. Sheng, W. C.; Zhuang, Z. B.; Gao, M. R.; Zheng, J.; Chen, J. G. G.; Yan, Y. S., Correlating hydrogen oxidation and evolution activity on platinum at different pH with measured hydrogen binding energy. *Nat Commun* **2015,** *6*.

3. Strmcnik, D.; Uchimura, M.; Wang, C.; Subbaraman, R.; Danilovic, N.; van der Vliet, D.; Paulikas, A. P.; Stamenkovic, V. R.; Markovic, N. M., Improving the hydrogen oxidation reaction rate by promotion of hydroxyl adsorption. *Nat Chem* **2013,** *5* (4), 300-306.
4. Durst, J.; Siebel, A.; Simon, C.; Hasche, F.; Herranz, J.; Gasteiger, H. A., New insights into the electrochemical hydrogen oxidation and evolution reaction mechanism. *Energ Environ Sci* **2014,** *7* (7), 2255-2260.
5. Xu, C.; Li, X.; Liu, T.; Zhang, H., Design and synthesis of a free-standing carbon nano-fibrous web electrode with ultra large pores for high-performance vanadium flow batteries. *RSC Advances* **2017,** *7* (73), 45932-45937.
6. Zheng, J.; Sheng, W.; Zhuang, Z.; Xu, B.; Yan, Y., Universal dependence of hydrogen oxidation and evolution reaction activity of platinum-group metals on pH and hydrogen binding energy. *Science Advances* **2016,** *2* (3).
7. Lu, S.; Zhuang, Z., Investigating the Influences of the Adsorbed Species on Catalytic Activity for Hydrogen Oxidation Reaction in Alkaline Electrolyte. *Journal of the American Chemical Society* **2017,** *139* (14), 5156-5163.
8. Davydova, E.; Mukerjee, S.; F., J.; Dekel, D. R., Electrocatalysts for hydrogen oxidation reaction in alkaline medium – A review. *Acs Catal* **2018,** *accepted*.
9. Zhuang, Z.; Giles, S. A.; Zheng, J.; Jenness, G. R.; Caratzoulas, S.; Vlachos, D. G.; Yan, Y., Nickel supported on nitrogen-doped carbon nanotubes as hydrogen oxidation reaction catalyst in alkaline electrolyte. *Nature Communications* **2016,** *7*, 10141.
10. Wang, H. S.; Abruna, H. D., IrPdRu/C as H-2 Oxidation Catalysts for Alkaline Fuel Cells. *J Am Chem Soc* **2017,** *139* (20), 6807-6810.
11. Qin, B.; Yu, H.; Jia, J.; Jun, C.; Gao, X.; Yao, D.; Sun, X.; Song, W.; Yi, B.; Shao, Z., A novel IrNi@PdIr/C core-shell electrocatalyst with enhanced activity and durability for the hydrogen oxidation reaction in alkaline anion exchange membrane fuel cells. *Nanoscale* **2018**.
12. Hossain, M. M.; Hou, J. Q.; Wu, L.; Ge, Q. Q.; Liang, X.; Mondal, A. N.; Xu, T. W., Anion exchange membranes with clusters of alkyl ammonium group for mitigating water swelling but not ionic conductivity. *J Membrane Sci* **2018,** *550*, 101-109.
13. Omasta, T. J.; Park, A. M.; Lamanna, J. M.; Zhang, Y.; Peng, X.; Wang, L.; Jacobson, D. L.; Varcoe, J. R.; Hussey, D. S.; Pivovar, B.; Mustain, W. E., Beyond catalysis and membranes: visualizing and solving the challenge of electrode water accumulation and flooding in AEMFCs. *Energ Environ Sci* **2018,** *11*, 551-558.
14. Dekel, D. R., Review of cell performance in anion exchange membrane fuel cells. *J Power Sources* **2018,** *375*, 158-169.
15. Lafforgue, C.; Chatenet, M.; Dubau, L.; Dekel, D. R., Accelerated Stress Test of Pt/C Nanoparticles in an Interface with an Anion-Exchange Membrane-An Identical-Location Transmission Electron Microscopy Study. *Acs Catal* **2018,** *8* (2), 1278-1286.
16. Matanovic, I.; Chung, H. T.; Kim, Y. S., Benzene adsorption: A significant inhibitor for the hydrogen oxidation reaction in alkaline conditions. *J. Phys. Chem. Lett.* **2017,** *8* (19), 4918-4924.
17. Maurya, S.; Fujimoto, C.; Hibbs, M. R.; Narvaez Villarrubia, C.; Kim, Y. S., Toward Improved Alkaline Membrane Fuel Cell Performance Using Quaternized Aryl-Ether Free Polyaromatics. *Chem. Mater.* **2018,** *30* (7), 2188-2192.
18. Unlu, M.; Abbott, D.; Ramaswamy, N.; Ren, X. M.; Mukerjee, S.; Kohl, P. A., Analysis of Double Layer and Adsorption Effects at the Alkaline Polymer Electrolyte-Electrode Interface. *J Electrochem Soc* **2011,** *158* (11), B1423-B1431.
19. Yim, S. D.; Chung, H. T.; Chlistunoff, J.; Kim, D. S.; Fujimoto, C.; Yang, T. H.; Kim, Y. S., A microelectrode study of interfacial reactions at the platinum-alkaline polymer interface. *Journal of the Electrochemical Society* **2015,** *162* (6), F499-F506.

20. Chung, H.; Choe, Y. K.; Martinez, U.; Gonzalez, I.; Mohanti, A.; Bae, C.; Kim, Y. S., Effect of Organic Cations on Hydrogen Oxidation Reaction of Carbon Supported Platinum. *J Electrochem Soc* **2016,** *163* (14), F1503-F1509.
21. Chung, H. T.; Martinez, U.; Chlistunoff, J.; Matanovic, I.; Kim, Y. S., Cation-hydroxide-water co-adsorption inhibits the alkaline hydrogen oxidation reaction. *Journal of Physical Chemistry Letters* **2016,** *7*, 4464-4469.
22. Dumont, J. H.; Hjelm, R.; Watkins, E. B.; Chung, H. T.; Martinez, U.; Atanassov, P.; Kim, Y. S., Investigating catalyst-electrolyte interface by microelectrode, infrared reflection adsorption spectroscopy and neutron relfectometry. In *PRiME 2016, 230th ECS meeeting*, The Electrochemical Society: Honolulu, Hawaii, 2016.
23. Alesker, M.; Page, M.; Shviro, M.; Paska, Y.; Gershinsky, G.; Dekel, D. R.; Zitoun, D., Palladium/nickel bifunctional electrocatalyst for hydrogen oxidation reaction in alkaline membrane fuel cell. *Journal of Power Sources* **2016,** *304*, 332-339.
24. Miller, H. A.; Lavacchi, A.; Vizza, F.; Marelli, M.; Di Benedetto, F.; Acapito, F. D. I.; Paska, Y.; Page, M.; Dekel, D. R., A Pd/C-CeO2 Anode Catalyst for High-Performance Platinum-Free Anion Exchange Membrane Fuel Cells. *Angew Chem Int Edit* **2016,** *55* (20), 6004-6007.
25. Miller, H. A.; Vizza, F.; Marelli, M.; Zadick, A.; Dubau, L.; Chatenet, M.; Geiger, S.; Cherevko, S.; Doan, H.; Pavlicek, R. K.; Mukerjee, S.; Dekel, D. R., Highly active nanostructured palladium-ceria electrocatalysts for the hydrogen oxidation reaction in alkaline medium. *Nano Energy* **2017,** *33*, 293-305.
26. Omasta, T. J.; Peng, X.; Miller, H. A.; Vizza, F.; Wang, L.; Varcoe, J. R.; Dekel, D. R.; Mustain, W. E., Beyond 1.0 W cm-2 performance without platinum – the beginning of a new era in anion exchange membrane fuel cells. *ACS Energy Letters* **2018,** *Submitted*.
27. Lee, W. H.; Park, E. J.; Han, J.; Shin, D. W.; Kim, Y. S.; Bae, C., Poly(terphenylene) Anion Exchange Membranes: The Effect of Backbone Structure on Morphology and Membrane Property. *ACS Macro Letters* **2017,** *6* (5), 566-570.
28. Hibbs, M. R., Alkaline Stability of Poly(phenylene)-Based Anion Exchange Membranes with Various Cations. *J Polym Sci Pol Phys* **2013,** *51* (24), 1736-1742.
29. Maurya, S.; Noh, S.; Matanovic, I.; Park, E. J.; Narvaez Villarrubia, C.; Han, J.; Bae, C.; Kim, Y. S., Rational design of polyaromatic ionomers for alkaline membrane fuel cells with >1 W cm-2 power density. **2018,** *Submitted*.
30. Krewer, U.; Weinzierl, C.; Ziv, N.; Dekel, D. R., Impact of carbonation processes in anion exchange membrane fuel cells. *Electrochim Acta* **2018,** *263*, 433-446.
31. Ziv, N.; Dekel, D. R., A practical method for measuring the true hydroxide conductivity of anion exchange membranes. *Electrochem Commun* **2018,** *88*, 109-113.
32. Perdew, J. P.; Chevary, J. A.; Vosko, S. H.; Jackson, K. A.; Pederson, M. R.; Singh, D. J.; Fiolhais, C., Atoms, Molecules, Solids, and Surfaces - Applications of the Generalized Gradient Approximation for Exchange and Correlation. *Phys Rev B* **1992,** *46* (11), 6671-6687.
33. Perdew, J. P.; Chevary, J. A.; Vosko, S. H.; Jackson, K. A.; Pederson, M. R.; Singh, D. J.; Fiolhais, C., Atoms, Molecules, Solids, and Surfaces - Applications of the Generalized Gradient Approximation for Exchange and Correlation (Vol 46, Pg 6671, 1992). *Phys Rev B* **1993,** *48* (7), 4978-4978.
34. Blochl, P. E., Projector Augmented-Wave Method. *Phys Rev B* **1994,** *50* (24), 17953-17979.
35. Kresse, G.; Joubert, D., From ultrasoft pseudopotentials to the projector augmented-wave method. *Phys Rev B* **1999,** *59* (3), 1758-1775.
36. Kresse, G.; Hafner, J., Abinitio Molecular-Dynamics for Liquid-Metals. *Phys Rev B* **1993,** *47* (1), 558-561.
37. Kresse, G.; Hafner, J., Ab-Initio Molecular-Dynamics Simulation of the Liquid-Metal Amorphous-Semiconductor Transition in Germanium. *Phys Rev B* **1994,** *49* (20), 14251-14269.
38. Kresse, G.; Furthmuller, J., Efficiency of ab-initio total energy calculations for metals and semiconductors using a plane-wave basis set. *Comp Mater Sci* **1996,** *6* (1), 15-50.

39. Kresse, G.; Furthmuller, J., Efficient iterative schemes for ab initio total-energy calculations using a plane-wave basis set. *Phys Rev B* **1996,** *54* (16), 11169-11186.
40. Hong, S.; Rahman, T. S., Adsorption and diffusion of hydrogen on Pd(211) and Pd(111): Results from first-principles electronic structure calculations. *Phys Rev B* **2007,** *75* (15).
41. Monkhorst, H. J.; Pack, J. D., Special Points for Brillouin-Zone Integrations. *Phys Rev B* **1976,** *13* (12), 5188-5192.
42. Methfessel, M.; Paxton, A. T., High-Precision Sampling for Brillouin-Zone Integration in Metals. *Phys Rev B* **1989,** *40* (6), 3616-3621.
43. Siebel, A.; Gorlin, Y.; Durst, J.; Proux, O.; Hasché, F.; Tromp, M.; Gasteiger, H. A., Identification of Catalyst Structure during the Hydrogen Oxidation Reaction in an Operating PEM Fuel Cell. *ACS Catal.* **2016,** *6* (11), 7326-7334.
44. Burke, L. D.; Casey, J. K., The Electrocatalytic Behavior of Palladium in Acid and Base. *J Appl Electrochem* **1993,** *23* (6), 573-582.
45. Grden, M.; Lukaszewski, M.; Jerkiewicz, G.; Czerwinski, A., Electrochemical behaviour of palladium electrode: Oxidation, electrodissolution and ionic adsorption. *Electrochim Acta* **2008,** *53* (26), 7583-7598.
46. Fujimoto, C.; Kim, D. S.; Hibbs, M.; Wrobleski, D.; Kim, Y. S., Backbone stability of quaternized polyaromatics for alkaline membrane fuel cells. *Journal of Membrane Science* **2012,** *423-424*, 438-449.
47. Choe, Y. K.; Fujimoto, C.; Lee, K. S.; Dalton, L. T.; Ayers, K.; Henson, N. J.; Kim, Y. S., Alkaline stability of benzyl trimethyl ammonium functionalized polyaromatics: A computational and experimental study. *Chemistry of Materials* **2014,** *26* (19), 5675-5682.
48. Mohanty, A. D.; Bae, C., Mechanistic analysis of ammonium cation stability for alkaline exchange membrane fuel cells. *Journal of Materials Chemistry A* **2014,** *2* (41), 17314-17320.
49. Dekel, D. R.; Arnar, M.; Willdorf, S.; Kosa, M.; Dhara, S.; Diesendruck, C. E., Effect of Water on the Stability of Quaternary Ammonium Groups for Anion Exchange Membrane Fuel Cell Applications. *Chem Mater* **2017,** *29* (10), 4425-4431.
50. Stanislaus, A.; Cooper, B. H., Aromatic Hydrogenation Catalysis - a Review. *Catal Rev* **1994,** *36* (1), 75-123.
51. Kim, D. S.; Fujimoto, C. H.; Hibbs, M. R.; Labouriau, A.; Choe, Y. K.; Kim, Y. S., Resonance Stabilized Perfluorinated Ionomers for Alkaline Membrane Fuel Cells. *Macromolecules* **2013,** *46* (19), 7826-7833.
52. Wang, L.; Maqliocca, E.; Cunningham, E. L.; Mustain, W. E.; Poynton, S. D.; Escudero-Cid, R.; Nasef, M. M.; Ponce-Gonzalez, J.; Bance-Souahli, R.; Slade, R. C. T.; Whelligan, D. K.; Varcoe, J. R., An Optimized Synthesis of High Performance Radiation-Grafted Anion-Exchange Membranes. *Green Chem* **2017**.